UNIVERSITÄT AUGSBURG
Universitätsbibliothek

OPEN ACCESS
OPUS AUGSBURG

Borosulfates hosting Se42+ ions —crystal structures, chemical bonding, optical spectroscopy, and magnetism

Erich Turgunbajew, Marios Symeonidis, Jörn Bruns, Sara N. Özbay, Jan Langwald, Mathias S. Wickleder, Robert E. Dinnebier, Linda S. Reitz, Richard Dronskowski, Lars Schumacher, Rainer Pöttgen, Henning A. Höppe

Angaben zur Veröffentlichung / Publication details:

Turgunbajew, Erich, Marios Symeonidis, Jörn Bruns, Sara N. Özbay, Jan Langwald, Mathias S. Wickleder, Robert E. Dinnebier, et al. 2026. "Borosulfates hosting Se42+ ions —crystal structures, chemical bonding, optical spectroscopy, and magnetism." *Angewandte Chemie International Edition* 65 (45): e4300417. https://doi.org/10.1002/anie.4300417.

Nutzungsbedingungen / Terms of use:

CC BY 4.0

Dieses Dokument wird unter folgenden Bedingungen zur Verfügung gestellt: / This document is made available under these conditions:
CC-BY 4.0: Creative Commons: Namensnennung
Weitere Informationen finden Sie unter: / For more information see:
https://creativecommons.org/licenses/by/4.0/deed.de

Check for updates

Angewandte Chemie International Edition

Angewandte International Edition Chemie

How to cite: *Angew. Chem. Int. Ed.* **2026**, 65, e4300417
doi.org/10.1002/anie.4300417

RESEARCH ARTICLE OPEN ACCESS Hot Paper

Borosulfates Hosting Se_4^{2+} Ions—Crystal Structures, Chemical Bonding, Optical Spectroscopy, and Magnetism

Erich Turgunbajew[1] | Marios Symeonidis[2] | Jörn Bruns[2] | Sara N. Özbay[3] | Jan Langwald[3] | Mathias S. Wickleder[3] | Robert E. Dinnebier[4] | Linda S. Reitz[5] | Richard Dronskowski[5] | Lars Schumacher[6] | Rainer Pöttgen[6] | Henning A. Höppe[1]

[1]Lehrstuhl für Festkörperchemie, Universität Augsburg, Augsburg, Germany | [2]Institut für Chemie, Technische Universität Berlin, Berlin, Germany | [3]Institut für Anorganische und Materialchemie, Universität zu Köln, Köln, Germany | [4]Röntgenographie, Max-Planck-Institut für Festkörperforschung, Stuttgart, Germany | [5]Institut für Anorganische Chemie, RWTH Aachen University, Aachen, Germany | [6]Institut für Anorganische und Analytische Chemie, Universität Münster, Münster, Germany

Correspondence: Henning A. Höppe (henning.hoeppe@uni-a.de)

Received: 13 July 2026 | **Revised:** 27 August 2026 | **Accepted:** 9 September 2026

Keywords: borosulfates | powder reflectance spectroscopy | selenium | thermal analysis | weakly coordinating anion

ABSTRACT

Despite consistent growth in the number of compounds known to host homo- and hetero polycations of group 16 elements, only two, $Se_4[HS_2O_7]_2$ and $Se_4[S_4O_{13}]$, provided an exclusively oxidic coordination environment, the former being the first structural characterization of the Se_4^{2+} cation in 1968. With the first selenium borosulfates $Se_4[B(S_2O_7)_2]_2(SO_3)$, $Se_4[B(S_2O_7)_2]_2$, $Se_4[B_2(SO_4)_2(S_2O_7)_2]$-I, $Se_4[B_2(SO_4)_2(S_2O_7)_2]$-II, and $Se_4[B_2(SO_4)_4]$ we extended this list by five compounds. Aside from $Se_4[HS_2O_7]_2$, $Se_4[S_4O_{13}]$ was synthesized but never structurally characterized. In this contribution we also evaluate the crystal structure of the tetrasulfate $Se_4[S_4O_{13}]$. All compounds are synthesized under solvothermal conditions. Powder reflectance spectra of the selenium borosulfates are in accordance with the yellow body color of the compounds. Magnetic measurements confirm the diamagnetic character of the Se_4^{2+} ions, in agreement with the calculations. Temperature-programmed powder X-ray diffraction reveals that the borosulfates of the study form sequentially with increasing decomposition temperature, enabling their selective synthesis. Furthermore, we performed infrared spectroscopy, Rietveld refinements and thermal analyses.

1 | Introduction

For a long time, strongly acidic and colorful solutions of chalcogens have fascinated chemists. As early as 1783, Müller von Reichenstein reported a solution showing an "unvergleichlich schöne gesättigte Karmoisinfarbe" – an incomparably beautiful, saturated crimson red color. This solution resulted from dissolving a metal, that he had extracted from a gold ore in sulfuric acid [1]. At that time, the element was still unknown and it took another 15 years until Klaproth confirmed the discovery of this new element which he then named tellurium [2]. In the early 19th century, Buchholz and Berzelius made similar observations when they dissolved the chalcogenides sulfur and selenium in sulfuric and selenic acid, respectively, yielding blue and yellow solutions [3–5]. The origin of the colored solutions remained mysterious for the following 150 years, despite numerous hypotheses regarding their nature [6–12]. Furthermore, the oxidation states of the chromophores were unknown, and the question whether the chromophores were radicals was controversially debated [10, 13–17]. This topic remained subject to discussion until Bjerrum

Dedicated to Professor Johannes Beck on the occasion of his 70th birthday.

This is an open access article under the terms of the Creative Commons Attribution License, which permits use, distribution and reproduction in any medium, provided the original work is properly cited.
© 2026 The Author(s). *Angewandte Chemie International Edition* published by Wiley-VCH GmbH

et al. and Gillespie et al. independently determined the color origin for tellurium and selenium in 1968. While Gillespie et al. investigated the origin of the colored species in highly acidic media like HSO_3F, $H_2S_2O_7$ and H_2SO_4, Bjerrum et al. chose the Lewis acidic molten salt $AlCl_3$-NaCl. Both proposed that the colors originate from polyatomic Se_4^{2+}, Se_8^{2+}, and Te_4^{2+} cations; still, their topology was unknown [18, 19]. In the same year, Gillespie et al. published the first compounds containing Se_4^{2+} cations in Brønsted acidic media including $Se_4[S_4O_{13}]$ and $Se_4[HS_2O_7]_2$. Later the year, the latter was subject to the first single crystal X-ray diffraction study, revealing the square planar shape of the cation [20–22]. Shortly thereafter, also the first tellurium and sulfur polycations were isolated in $Te_x[AlCl_4]$ [23] and $S_8[AsF_6]_2$ [24] by Corbett and Gillespie. Over the following years, more complex chalcogen homo– and heteropolyatomic cations also mixing elements of main-groups V through VII, were isolated in solids. In this context, the contributions to this topic by the group of Johannes Beck ought be highlighted [25–28]. Intriguingly, while these cations were initially found in Brønsted acidic media, the stabilization in the subsequent studies almost exclusively occurred in fluorido-antimonates and -arsenates and other halidometallates [29, 30]. Until this year, $Se_4[HS_2O_7]_2$ and $Se_4[S_4O_{13}]$ remained the only purely oxoanionic compounds known to stabilise these polycations, whereby a recent contribution by Wickleder et al. brought a deeper insight into the stabilizing potential of oxoanions towards the Ch_4^{2+} (*Ch* = Se, Te) cations as well as Te_6^{4+} [31].

The conjugated bases of strong Brønsted and Lewis acids exhibit weak coordination behavior that appears to be a precondition for the stabilization of such cations. In 1971, Gillespie determined the Hammett acidity function for several selected acidic systems including the $H_2SO_4/HB(HSO_4)_4$ system. Hence, the H_0 values were determined to be approximately –13, on par with HSO_3F, characterizing borosulfonic acid as superacidic [32]. Accordingly, the deprotonated anion $[B(SO_4)_4]^{5-}$ provides a weak coordination. Today, this anion is regarded as the typical basic building unit of borosulfates, a comparably new material class with their first crystallographically characterized representative $K_5[B(SO_4)_4]$ published in 2012 [33]. Borosulfates typically constitute of alternating sulfate and borate tetrahedra sharing common vertices to produce zero-, as in $Li_5[B(SO_4)_4]$ [34], one-, as in $Ag[B(SO_4)_2]$ [35], two- as in $Cd[B_2(SO_4)_4]$ [36], and three-dimensional anions like in $Li[B(SO_4)_2]$ [37]. The weak coordination strength of borosulfates was reported several times. For instance, diffuse reflectance spectra of α-$M_4[B_2O(SO_4)_6]$ (M = Co, Ni) revealed small Racah parameters and ligand field splitting compared to their respective sulfates and chlorides [38]. Additionally, luminescence spectroscopy of $Ce_2[B_2(SO_4)_6]$ unveiled emissions deep in the UV regime comparable to fluorides [39]. Recently, ^{121}Sb Mössbauer spectra of $SbA[B(SO_4)_2]_4$ (A = K, Rb, Cs, NH_4) revealed the most negative isomer shift to date of almost –22 mm·s^{-1}, confirming the anion´s weak coordination strength [40]. Additionally, in $I_4[B(S_2O_7)_2]_2$ the structurally related homopolycation I_4^{2+} was stabilized, previously only reported in weakly coordinating anions like fluoridoantimonates [41].

The research on these homo- and heteropolycations of the elements in the main groups V, VI, and VII mainly focused on the discovery, their synthesis, stabilization and structural analysis of new polycations in metal halides, and their theoretical treatment. If any further investigations on the properties of the cations were carried out, these were typically performed in solution. Herein, we present five borosulfates and a polysulfate containing Se_4^{2+} ions in a purely oxoanionic coordination environment. We elucidate their crystal structures and, for the first time, present UV–vis spectra of Se_4^{2+} cations in solids. Furthermore, we performed thermogravimetric analyses (TGA) and temperature programmed powder X-ray diffraction (TPPXRD) experiments highlighting the structural relationship between all presented borosulfates. These results are complemented by DFT calculations, infrared spectroscopy (IR) and magnetic measurements.

2 | Results and Discussion

2.1 | Crystal Structures $Se_4[S_4O_{13}]$

Elemental selenium dissolved in oleum (65% SO_3) at room temperature leads to the formation of selenium hydrogendisulfate $Se_4[HS_2O_7]_2$, already shown by Gillespie et al. in the 1960´s [20]. The Wickleder group focuses on the synthesis of polysulfates and found that, while SO_3-rich oleum (65% SO_3) typically only results in disulfates, using neat SO_3 enhances the formation of polysulfates with higher condensation degrees, reaching up to hexasulfates like $(NH_4)_2[S_6O_{19}]$ and $Rb_2[S_6O_{19}]$ which constitute the longest polysulfates known till date [42]. With $Se_4[S_4O_{13}]$ we introduce a new representative comprising the still quite rare tetrasulfate $[S_4O_{13}]^{2-}$ anion (Figure 1a). The latter was first reported only a decade ago along with the synthesis of $(NO_2)_2[S_4O_{13}]$ [43]. Even though the composition of $Se_4[S_4O_{13}]$ was already determined accurately by a gravimetric analysis in 1968 by Gillespie et al., its structure remained unknown – until now [20]. $Se_4[S_4O_{13}]$ crystallizes in the orthorhombic space group $P2_12_12_1$ (no. 19) with eight formula units per unit cell – and due to the weak coordination strength of the polysulfate intrinsically as inversion twin, though. The structure consists of two crystallographically independent tetrasulfate anions arranged in a strongly distorted fcc-like manner where the Se_4^{2+} rings fill the octahedral voids and are coordinated by seven tetrasulfate anions each (Figure 1). The latter are present in a zig zag arrangement with a dihedral angle close to 180°. This is in line with the observed sulfate chain conformation within the halogen tetrasulfates $(IX_2)_2[S_4O_{13}]$ (X = Br, I) recently reported by Wickleder et al. [44]. Contrarily, group I and II tetrasulfates show (except the hydrogenium-*bis*-tetrasulfate anion $[H(S_4O_{13})_2]^{3-}$), a predominantly horseshoe-type arrangement [45]. A direct comparison between both conformations is shown in the supplement (Figure S1). The bond lengths in the anion are comparable to the lithium compound $Li_2[S_4O_{13}]$: terminal S–O bonds range between 141 and 144 pm, whereas the S–O–S bridges exhibit a bond length asymmetry, that is alternating long and short bonds between 154 and 175 pm (Table S7), which we also analyzed previously. The terminal S–O bonds coordinating towards the Se_4^{2+} cation show the largest bond extension and the strongest distortion of the sulfur centre towards a tetrahedral geometry, due to strong non-covalent interactions with the cation. Notably, the observed terminal bond lengths and sulphate geometries indicate that the Lewis acidity of the Se_4^{2+} cation is in the same order of magnitude as for the Li^+ cation.

15213773, 2026, 45, Downloaded from https://onlinelibrary.wiley.com/doi/10.1002/anie.430417 by Universitätsbibliothek Augsburg, Wiley Online Library on [08/11/2026]. See the Terms and Conditions (https://onlinelibrary.wiley.com/terms-and-conditions) on Wiley Online Library for rules of use; OA articles are governed by the applicable Creative Commons License

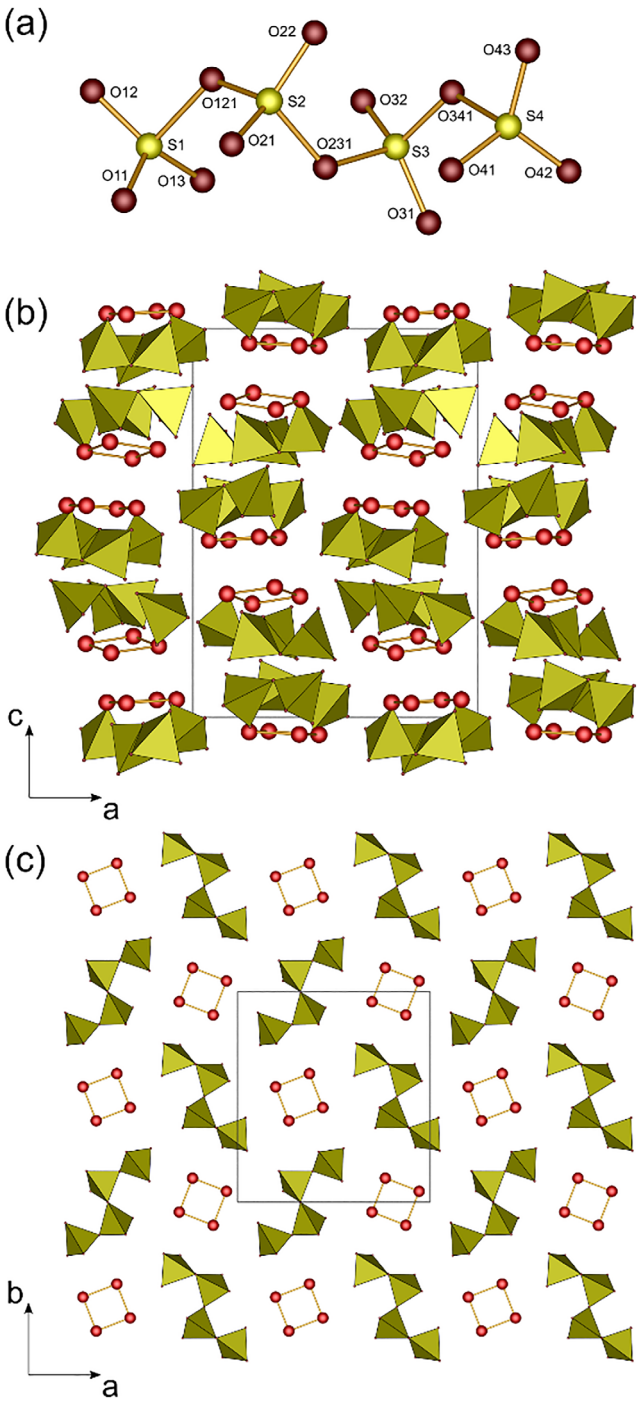


FIGURE 1 | (a) $S_4O_{13}^{2-}$ unit of $Se_4[S_4O_{13}]$. (b, c) Unit cell of $Se_4[S_4O_{13}]$ along different directions. For a better understanding of the structural arrangement in (b) only a single layer is displayed.

2.2 | $Se_4[B(S_2O_7)_2]_2(SO_3)$

While the reactions in neat SO_3 and oleum (65% SO_3) at moderate temperatures typically lead to polysulfates as discussed above, adding boron oxide to such reactions typically yields unconventional borosulfates featuring $(S_2O_7)^{2-}$ units with S–O–S bridges. Consequently, in this study four such borosulfates were prepared. The first, $Se_4[B(S_2O_7)_2]_2(SO_3)$, crystallizes in the monoclinic space group *C*2/*c* (no. 15) with four formula units per unit cell (Figure 2). This structure can be derived from the AlB_2 structure type where the $[B(S_2O_7)_2]^{2-}$ units resemble the graphene-like boron layers and the selenium cations occupy all hexagonal prismatic sites (Figure S2). Subsequently, each Se_4^{2+} cation is coordinated by twelve $[B(S_2O_7)_2]^{2-}$ anions and two additional SO_3 molecules, located between adjacent Se_4^{2+} cations. The $[B(S_2O_7)_2]^-$ anion is well known in literature occurring with simple mono- and divalent cations like in $A[B(S_2O_7)_2]$ (A = Li, Na, K, NH_4, Ag) [34, 37, 46, 47] and $Ba[B(S_2O_7)_2]_2$ [48] but also more exotic oligocations like in the aforementioned $I_4[B(S_2O_7)_2]_2$ [41] and $[Au_2Cl_4][B(S_2O_7)_2](SO_3)$ [49]. Within the anion we deduced typical bond lengths, comparable to the previously mentioned compounds featuring *bis*–disulfatoborate anions (Table S5).

2.3 | $Se_4[B(S_2O_7)_2]_2$

The SO_3 molecule in $Se_4[B(S_2O_7)_2]_2(SO_3)$ is bound quite weakly and can be readily removed to give $Se_4[B(S_2O_7)_2]_2$. By storing the SO_3-rich modification for a few days in a glovebox, the removal already occurs at room temperature and is completed after a few weeks. The $Se_4[B(S_2O_7)_2]_2$ structure was solved from powder X-ray diffraction data (details in the Supporting Information) and crystallizes in the monoclinic space group *C*2/c (no. 15) with four formula units per unit cell. Despite a reorientation of the molecular ions, the coordination number for the Se_4^{2+} cations as well as the structural motifs with their AlB_2-type arrangement are retained, where the Se_4-units occupy the Al and $[B(S_2O_7)_2]^-$ anions replace the B positions. As expected, the loss of SO_3 results in a shrunk unit cell (Figures 2b,d, Table S2). All bond lengths remain in the expected range (Table S5).

2.4 | $Se_4[B_2(SO_4)_2(S_2O_7)_2]$-I

Two polymorphs fulfil the composition $Se_4[B_2(SO_4)_2(S_2O_7)_2]$. $Se_4[B_2(SO_4)_2(S_2O_7)_2]$-I adopts space group $P2_1/c$ (no. 14) with two formula units per unit cell and comprises Se_4^{2+} cations and zero-dimensional $[B_2(SO_4)_2(S_2O_7)_2]^{2-}$ units. These units constitute a new anion topology for borosulfates; it can be considered as a modification of the cyclic anion found in the rare-earth borosulfate series $R_2[B_2(SO_4)_6]$ (R = Y, La–Nd, Sm–Lu) [39] where two of the four terminal (SO_4) units condense to two chelating (S_2O_7) units. Hence, the two boron atoms are bridged by two (SO_4) groups forming *vierer* rings and additionally are coordinated by a chelating (S_2O_7) unit each. Consequently, according to Liebau´s nomenclature the anion is defined as a loop-branched *vierer* single ring [50]. All observed bond lengths agree with the sum of the ionic radii and other borosulfates featuring S–O–S bridges (Table S5). As illustrated in Figure 3, viewing along the *a*-direction, the Se_4^{2+} cations as well as the $[B_2(SO_4)_2(S_2O_7)_2]^{2-}$ anions, form close packed layers even though these are not packed alike hcp where the spheres of layer B are situated above the triangles of spheres of layer A; here the Se_4^{2+} cations lie above and below parallelograms formed by $[B_2(SO_4)_2(S_2O_7)_2]^{2-}$ anions leading to an eightfold coordination by the latter.

15213773, 2026, 45, Downloaded from https://onlinelibrary.wiley.com/doi/10.1002/anie.430047 by Universitätsbibliothek Augsburg, Wiley Online Library on [08/11/2026]. See the Terms and Conditions (https://onlinelibrary.wiley.com/terms-and-conditions) on Wiley Online Library for rules of use; OA articles are governed by the applicable Creative Commons License

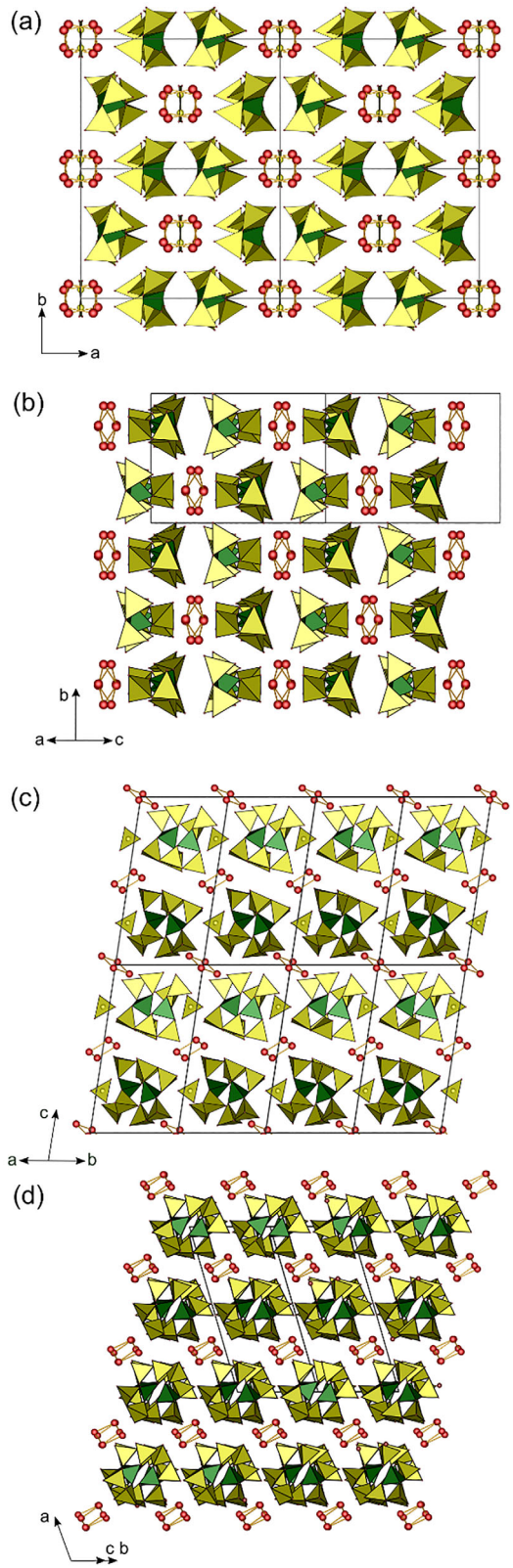


FIGURE 2 | Comparison of the structures of $Se_4[B(S_2O_7)_2]_2(SO_3)$ (a + c) and $Se_4[B(S_2O_7)_2]_2$ (b + d) along two different viewing directions.

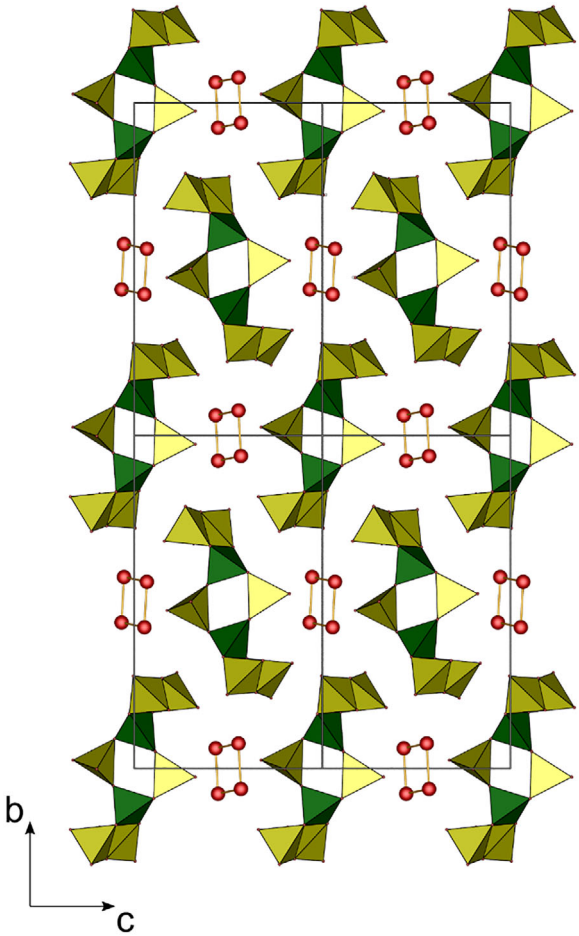


FIGURE 3 | 2×2 unit cells of $Se_4[B_2(SO_4)_2(S_2O_7)_2]$–I viewed along [100].

2.5 | $Se_4[B_2(SO_4)_2(S_2O_7)_2]$-II

The second polymorph of $Se_4[B_2(SO_4)_2(S_2O_7)_2]$ crystallizes also in space group type $P2_1/c$ (no. 14) as the first one and exhibits four formula units per unit cell. Contrarily, it features a one-dimensional anion instead, known from $A[B(SO_4)(S_2O_7)]$ (A = Cs, H) and the recently published $Pd[B(SO_4)(S_2O_7)]_2$ (Figure 4a) [46, 51]. Similarly, to the first polymorph, the central boron atoms are coordinated by two (SO_4) and a chelating (S_2O_7) subunit. Compared to the first polymorph, however, where both (SO_4) units coordinate to the same boron atom to form *vierer* single rings, these rings are opened to coordinate two distinct boron atoms and hence form chains running along the [100] direction (Figure 4b). These chains can be described as loop-branched *vierer* single chains. The observed bond lengths agree well with other borosulfates (Table S5). Charge compensation is achieved by one crystallographically independent Se_4^{2+} cation, coordinated by four chains each.

2.6 | $Se_4[B_2(SO_4)_4]$

$Se_4[B_2(SO_4)_4]$ crystallizes in space group $C2/c$ (no. 15) with two formula units per unit cell (Figure 5). Alternating borate and sulfate tetrahedra share common corners and form chains running along [010], analogous to SiS_2 (Si → B, S → SO_4). While

15213773, 2026, 45, Downloaded from https://onlinelibrary.wiley.com/doi/10.1002/anie.430417 by Universitätsbibliothek Augsburg, Wiley Online Library on [08/11/2026]. See the Terms and Conditions (https://onlinelibrary.wiley.com/terms-and-conditions) on Wiley Online Library for rules of use; OA articles are governed by the applicable Creative Commons License

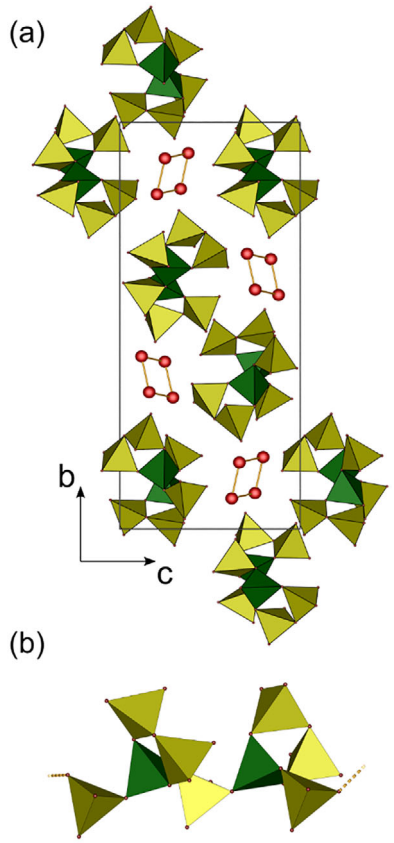


FIGURE 4 | (a) Unit cell viewed along [100] and (b) the fundamental building unit of $Se_4[B_2(SO_4)_2(S_2O_7)_2]$-II.

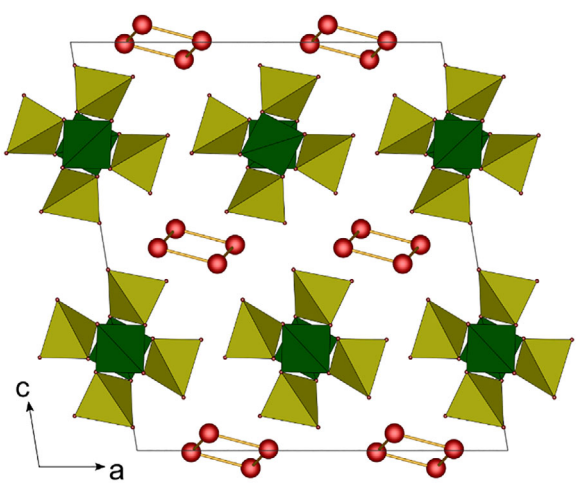


FIGURE 5 | Unit cell of $Se_4[B_2(SO_4)_4]$ viewed along [010].

each borate is connected to four adjacent sulfate tetrahedra each sulfate tetrahedron connects two borate tetrahedra forming *vierer* rings. Accordingly, the anion can be described as loop branched *vierer* single chains exhibiting the Niggli formula $_\infty^1\{[B(SO_4)_{4/2}]^-\}$. This anion topology is common to borosulfate chemistry and found for example in $A[B(SO_4)_2]$ (A = H_3O, NH_4, K, Ag) [34, 35, 46] and $M[B(SO_4)_2]$ (M = Sr, Pb, Ba) [48, 52, 53]. A comparison of these compounds with $Se_4[B_2(SO_4)_4]$ reveals a clear difference in the arrangement of the chains. It is evident that the chains tilt to accommodate the cations' size and non-spherical shape. The

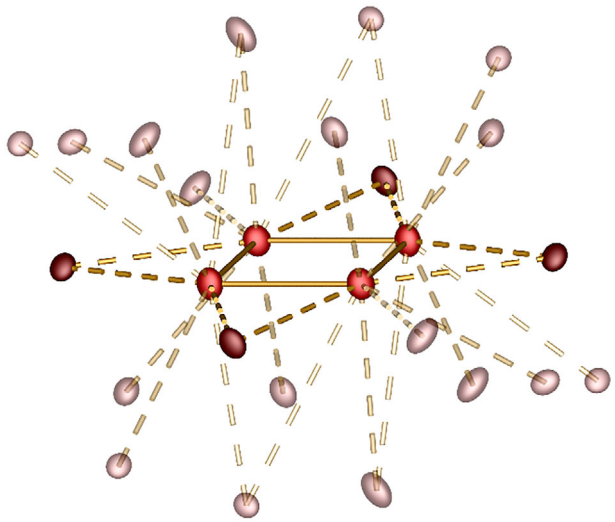


FIGURE 6 | Typical coordination environment of Se_4^{2+} in borosulfates exemplified by $Se_4[B_2(SO_4)_4]$. The oxygen atoms coordinating the edges of the rings are highlighted. Oxygen atoms in dark red; selenium in red. Displacement ellipsoids are set to 70% probability.

selenium rings are stacked along [100] and coordinated by four chains each. All observed bond lengths in the (BO_4) and (SO_4) tetrahedra are typical for compounds with this structural motif and are presented in Table S5.

The coordination environment of the Se_4^{2+} cations in all six compounds resembles the specifics of Ch_4^{2+} cations (Ch = chalcogen) and is exemplified in Figure 6 for $Se_4[B_2(SO_4)_4]$ while the remaining ones are depicted in the Figure S3. The shortest contacts are consistently observed to four oxygen atoms bridging the edges of the Se_4^{2+} square with mean values between 272 and 293 pm. The total coordination number (CN) was confirmed via MAPLE calculations (Madelung Part of Lattice Energy) and ranges between 17 for $Se_4[B_2(SO_4)_2(S_2O_7)_2]$-II and 20 for $Se_4[S_4O_{13}]$ considering a threshold of 370 pm (Tables S8-S13) [54–58]. These high coordination numbers are common for smaller coordinating atoms like oxygen and fluorine and decrease with rising ionic radii in chlorides and bromides. Not only does the size and hence electron density influence the CN but also the coordination strength and the bond lengths within the cation; even the color of the compound correlates with the CN. Based on the limited number of compounds known at the time, Burns et al. concluded that increasing polarizability or, alternatively increasing its charge density, strengthens the cation-anion interactions leading to a bond elongation. Hence, the energy gap in Se_4^{2+} between the HOMO and LUMO formed by the selenium p-orbitals decreases and the color of the compounds shifts from yellow to orange [59, 60]. Table 1 lists the mean Se–Se distances as well as the color of the compounds containing Se_4^{2+} ions; here, only compounds were included where the color can reasonably be attributed to the Se_4^{2+} cations. We can confirm the general trend that with increasing Se–Se distance a shift from yellow over orange to red is observed. Albeit this rule does not hold strictly, for example $Se_4[S_4O_{13}]$ and $Se_4[AlCl_4]_2$. Although $Se_4[S_4O_{13}]$ exhibits an average bond length greater than $Se_4[AlCl_4]_2$, the former is yellow while the latter shows an orange hue (Table 1). The statistical error of these averaged bond lengths

15213773, 2026, 45, Downloaded from https://onlinelibrary.wiley.com/doi/10.1002/anie.430417 by Universitätsbibliothek Augsburg, Wiley Online Library on [08/11/2026]. See the Terms and Conditions (https://onlinelibrary.wiley.com/terms-and-conditions) on Wiley Online Library for rules of use; OA articles are governed by the applicable Creative Commons License

TABLE 1 | Mean Se–Se distances and color appearance of Se_4^{2+} cations in $Se_4[S_4O_{13}]$, $Se_4[B(S_2O_7)_2]_2(SO_3)$, $Se_4[B(S_2O_7)_2]_2$, $Se_4[B_2(SO_4)_6]$, $Se_4[B_2(SO_4)_2(S_2O_7)_2]$-I, and $Se_4[B_2(SO_4)_2(S_2O_7)_2]$-II compared to compounds reported previously

Compound	Mean Se–Se distance / pm	Se-distance range / pm	Point group	Color appearance	Ref.
$Se_4[Sb_2F_4][Sb_2F_5][SbF_6]_5$	226.1(6)	224.7-227.6	D_{2h}	yellow	[61]
$Se_4[SbF_{17}][SbF_6]_3$	227.2(5)	226.5-227.5	D_{2h}	yellow	[62]
$Se_4[B_2(SO_4)_4]$	227.95(6)	227.9-228.0	D_{2h}	yellow	this work
$Se_4[B_2(SO_4)_2(S_2O_7)_2]$-II	228.08(8)	227.6-228.7	C_1	yellow	this work
$Se_4[HS_2O_7]_2$	228.3(6)	228.0-228.6	D_{2h}	orange	[20]
$Se_4[B_2(SO_4)_2(S_2O_7)_2]$-I	228.49(8)	228.1-228.9	D_{2h}	yellow	this work
$Se_4[B(S_2O_7)_2]_2(SO_3)$	228.53(6)	228.5-228.6	D_{2h}	yellow	this work
$Se_4[AlCl_4]_2$	228.5(2)	228.3-228.8	D_{2h}	orange	[61]
$Se_4[Bi_6F_{11}][AsF_6]_9 \cdot 10\ SO_2$	228.8(2)	228.1-229.5	D_{2h}	yellow	[63]
$Se_4[S_4O_{13}]$	228.9(1)	228.5-229.2	C_1	yellow	this work
$Se_4[S_2O_7]$	228.57(3)	228.1-229.1	C_1	orange	[31]
$Se_4[HS_3O_{10}]$	228.62(3)	228.5-228.8	C_i	yellow	[31]
$Se_4[HfCl_6]$	229.18(9)	229.2	D_{2h}	light red	[64]
$Se_4[ZrCl_6]$	229.7(3)	229.2-230.1	D_{2h}	light red	[64]
$Se_4[Bi_4Cl_{14}]$	229.6(1)	229.6	D_{4h}	red	[65]

is based on the esds of the refinements. Accordingly, the color hue of the compounds is a more reliable indicator for the coordination strength of a host structure than considering the mean Se–Se distances only. Thus, exhibiting a yellow body, the tetrasulfate and borosulfate anions reported in this study can be considered at least as weakly coordinating as the compound class of fluoridoantimonates. Regarding the molecular cations, all Se_4^{2+} rings within the borosulfates exhibit mean bond lengths between 227.95(6) and 228.53(6) pm ranking approximately between the fluorides and chlorides (Table 1); moreover, the Se_4^{2+} cations only slightly deviate from D_{4h} symmetry. Detailed geometrical data are listed in the Table S6. All compounds were synthesised as phase pure crystalline powders (Figures S5–S10).

2.7 | Chemical Bonding in $Se_4[B_2(SO_4)_4]$

To shed some quantum-chemical light on the bonding situation, especially in the Se_4-unit, the crystal structure of $Se_4[B_2(SO_4)_4]$ was DFT-optimized and the resulting wavefunctions were projected onto a local atomic-orbital basis using the LOBSTER suite. This procedure allowed us to calculate a local DOS, precise bond orders and a molecular orbital scheme of the Se_4-unit [66]. All computational details are provided in the Supporting Information.

Figure 7a shows the total DOS. The most significant contributions stem from the oxygen's 2s and 2p, the selenium's 4p and sulfur's 3p orbitals. The calculated Löwdin charges (Figure 7b) are provided next to the corresponding atoms in the $Se_4[B_2(SO_4)_4]$ unit. The integrated charge for the Se_4-unit is +1.64 which is close to the ionic-limit value of +2. Both, the sulfur and boron atoms are coordinated tetrahedrally by oxygen. The Löwdin charge on the oxygen atoms surrounding boron amounts to −0.70. The terminal oxygen atoms of the sulfate tetrahedra show a Löwdin charge of −0.90.

To better understand the bonding of the Se_4-unit, the two-centre as well as the four-centre Crystal Orbital Bond Indices (COBI) were calculated [67]. The COBI as well as the corresponding integrated values (ICOBI) are provided in Figures 7c,d. Since the two-centre ICOBI directly corresponds to the bond order, the $ICOBI^{(2)}$ values of 1.11 for the two types of Se–Se bonds in the Se_4-unit show that these bonds can be understood as covalent single bonds. The four-centre $ICOBI^{(4)}$ value given in the right part of the Figure shows that there is also a significant four-centre interaction, some delocalisation across the ring. The highest orbital-wise contribution to this interaction of a $4p_z$ $^{4pz\ 4pz}$ $4p_z$ character. Here, the $4p_z$ orbitals are arranged perpendicular to the bonds in the Se_4 unit.

LOBSTER also allows for the calculation of molecular (instead of atomic) orbitals of a defined molecular unit [68]. The MO-DOS as well as the MO-scheme with the corresponding molecular orbitals for the Se_4 unit are given in Figure 8b. An even more detailed MO-scheme is presented in Figure 8d to show the atomic-orbital contributions to the MOs. The molecular orbital formation energy (MOFE) in Figure 8c can be understood as a COHP analogue that is partitioning of the Kohn-Sham energy but molecular-orbital like. Hence, MOFE measures the energetic contribution of each atomic orbital to a molecular orbital, plotted here such that bonding MOs appear to the right of Figure 8c and antibonding MOs to the left. The integrated MOFE values (IMOFE) corresponding to the diverse interactions forming the molecular orbitals are also provided in Figure 8c.

15213773, 2026, 45, Downloaded from https://onlinelibrary.wiley.com/doi/10.1002/anie.430417 by Universitätsbibliothek Augsburg, Wiley Online Library on [08/11/2026]. See the Terms and Conditions (https://onlinelibrary.wiley.com/terms-and-conditions) on Wiley Online Library for rules of use; OA articles are governed by the applicable Creative Commons License

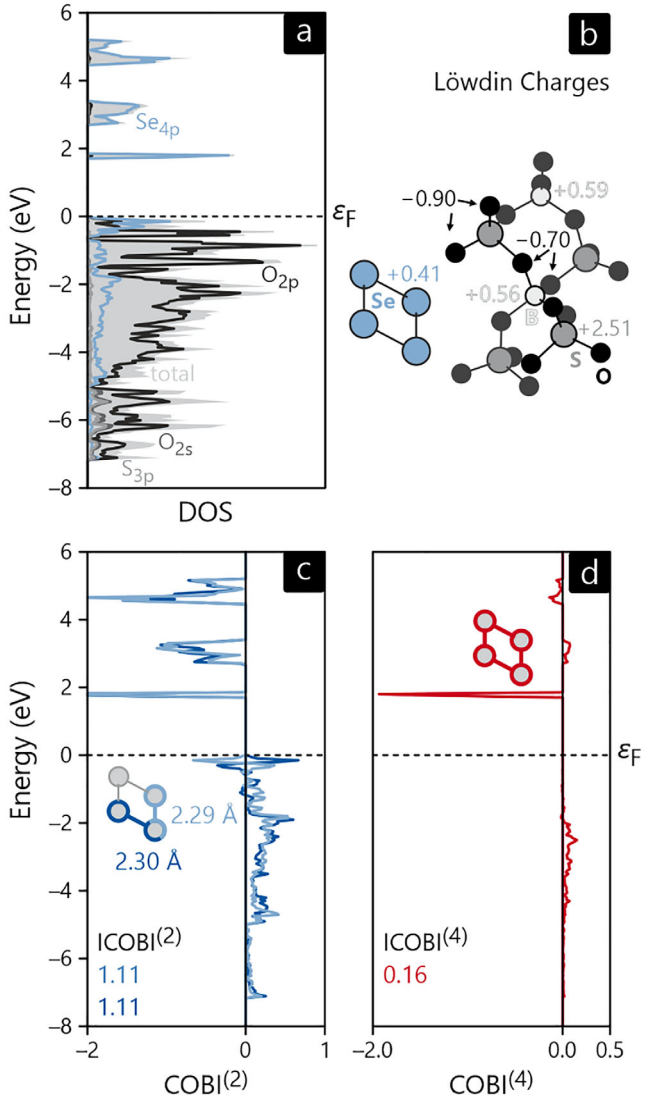


FIGURE 7 | (a) Total-DOS shown in light grey with the most significant contribution from oxygen's 2s and 2p (highlighted in dark grey and black) selenium's 4p (blue) and sulfur's 3p (grey) orbitals. (b) Schematic depiction of a $Se_4[B_2(SO_4)_4]$ unit with the charges for each species. Plots of the Crystal Orbital Bond Index for (c) two and (d) four centres are provided with their corresponding integrated (ICOBI) values.

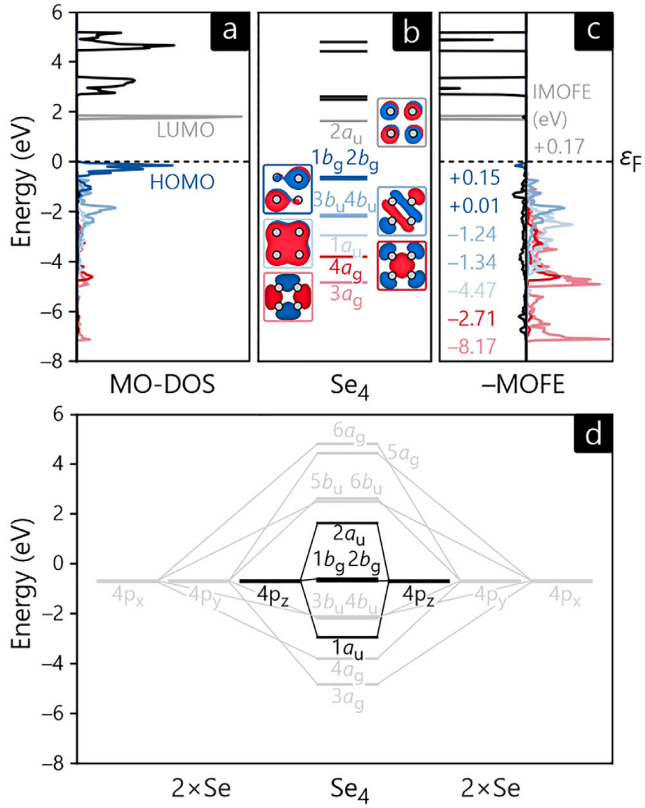


FIGURE 8 | (a) Molecular Orbital-resolved DOS, (b) Molecular Orbital (MO) scheme with visualized molecular orbitals, (c) MOFE diagram with IMOFE values for the Se_4-unit and (d) MO scheme with AO contributions.

TABLE 2 | MO–energy, IMOFE, and Löwdin gross orbital population (GOP) for the Se_4-unit

Molecular Orbital	MO energy (eV)	IMOFE (eV)	Löwdin GOP
$2a_u$	+1.63	+0.17	0.07
$2b_g$	−0.60	+0.15	1.99
$1b_g$	−0.69	+0.01	1.99
$4b_u$	−2.12	−1.24	1.99
$3b_u$	−2.19	−1.34	1.99
$1a_u$	−2.94	−4.47	1.98
$4a_g$	−3.80	−2.71	1.97
$3a_g$	−4.83	−8.17	1.99

A more detailed analysis of the MOFE diagram in Figure 8c reveals that the $1b_g$ and $2b_g$ levels between −2 eV and the valence-band maximum appear on the left side of the plot indicating a slightly antibonding/nonbonding character. The corresponding IMOFE values of +0.15 eV and +0.01 eV reveal a minor destabilization caused by the formation of these molecular orbitals. These levels can be assigned to the selenium "lone pairs", which show up as the HOMO levels of the Se_4 unit. The more detailed MO scheme in Figure 8d yields that the $1b_g$ and $2b_g$ are formed by the $4p_z$ orbitals and have a π-character. The $4p_z$ orbitals also form two additional π-character MOs. These are the $1a_u$ as well as the antibonding $2a_u$. The Löwdin gross population of the Se_4-unit (Table 2) shows that this unit follows the *Aufbau principle* as indicated by the doubly occupied valence levels below the Fermi level and (almost) empty conduction levels.

2.8 | Magnetic Susceptibility Studies

The temperature-dependent magnetic susceptibilities of $Se_4[B(S_2O_7)_2]_2(SO_3)$ and $Se_4[S_4O_{13}]$ are shown in Figure 9. Both compounds are diamagnetic over the whole temperature range with room temperature values of $-6(1) \times 10^{-4}$ emu mol^{-1} for $Se_4[B(S_2O_7)_2]_2(SO_3)$ and $-6.0(2) \times 10^{-4}$ emu mol^{-1} for $Se_4[S_4O_{13}]$. The susceptibility increase at low temperatures can be attributed to tiny amounts of paramagnetic impurities (so-called Curie tails). The $Se_4[B(S_2O_7)_2]_2(SO_3)$ sample seems to

15213773, 2026, 45, Downloaded from https://onlinelibrary.wiley.com/doi/10.1002/anie.430417 by Universitätsbibliothek Augsburg, Wiley Online Library on [08/11/2026]. See the Terms and Conditions (https://onlinelibrary.wiley.com/terms-and-conditions) on Wiley Online Library for rules of use; OA articles are governed by the applicable Creative Commons License

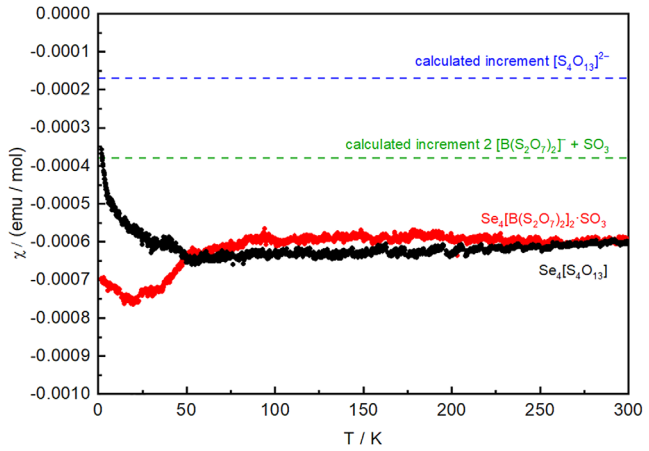


FIGURE 9 | Temperature dependence of the magnetic susceptibilities of $Se_4[B(S_2O_7)_2]_2(SO_3)$ and $Se_4[S_4O_{13}]$ measured with an applied external magnetic field of 10 kOe. For comparison, the summed diamagnetic increments [69] for $[S_4O_{13}]^{2-}$ and $2[B(S_2O_7)_2]^- + SO_3$ are shown by dotted lines.

have an additional diamagnetic impurity that shows up below 50 K, most likely arising from the reaction with the capsule (*vide ultra*).

To classify the room temperature values of $Se_4[B(S_2O_7)_2]_2(SO_3)$ and $Se_4[S_4O_{13}]$, we compare the experimental data with the sums of diamagnetic increments [69]. Since no increment is available for the Se_4^{2+} cation, we calculated the sums for the anions $[S_4O_{13}]^{2-}$ and $2[B(S_2O_7)_2]^- + SO_3$. These values are drawn as dotted lines in Figure 9. They are of the same order of magnitude as the experimental ones. The diamagnetic contributions of the Se_4^{2+} cations then push the susceptibilities to lower values, hence in good agreement between the experimental values and the increments.

2.9 | Optical Spectroscopy

To quantify the yellow color of the compounds, we recorded powder reflectance spectra of $Se_4[B(S_2O_7)_2]_2$, $Se_4[B_2(SO_4)_2(S_2O_7)_2]$-I, $Se_4[B_2(SO_4)_2(S_2O_7)_2]$-II, and $Se_4[B_2(SO_4)_4]$ from 200 to 750 nm (Figure 10). The spectra are dominated by three very intense broad bands with one ranging up to 500 nm into the visible regime; this is consistent with the yellow color of the powders based on a strong absorption in the blue to violet regime. These broad bands originate from $\pi^* \leftarrow \pi$ transitions within Se_4^{2+} and agree well with results of the DFT calculations for $Se_4[B_2(SO_4)_4]$ considering the systematic underestimation of the band gap by this method (up to 40%). The first absorption band peaking around 450 nm can be assigned to a $2a_u \leftarrow 2b_g/1b_g$ transition while the transition around 330 nm can be assigned to the $5b_u/6b_u \leftarrow 2b_g/1b_g$ transition. Spectroscopic data on Se_4^{2+} cations in solid samples are scarce, as listed in Table 3 [18, 60]. With absorption maxima located between 440 to 460 nm the coordination strength of borosulfates resembles that of hexafluoridoarsenates. A comparison between the spectra shows a small red shift from $Se_4[B(S_2O_7)_2]_2$ to $Se_4[B_2(SO_4)_4]$. These results are in accordance with earlier findings in borosulfates where compounds with terminal disulfate groups compared to solely sulfate groups show a slightly weaker coordination

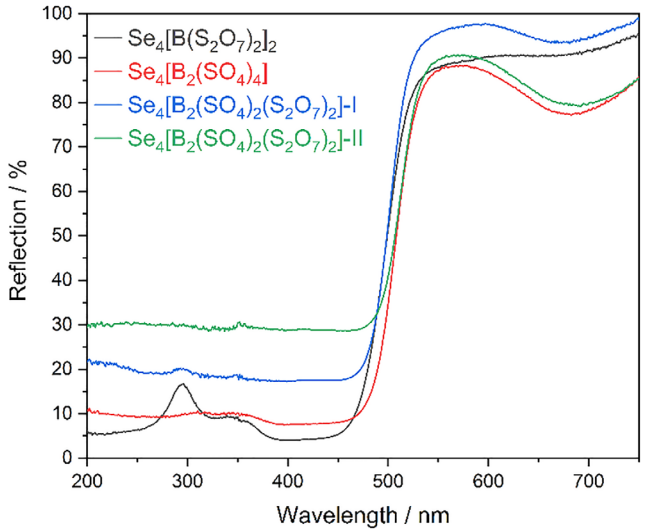


FIGURE 10 | Powder reflectance spectra of $Se_4[B(S_2O_7)_2]_2$ (black), $Se_4[B_2(SO_4)_4$ (red), $Se_4[B_2(S_2O_7)_2(SO_4)_2]$-I (blue) and $Se_4[B_2(S_2O_7)_2(SO_4)_2]$-II (green) recorded between 200 and 750 nm.

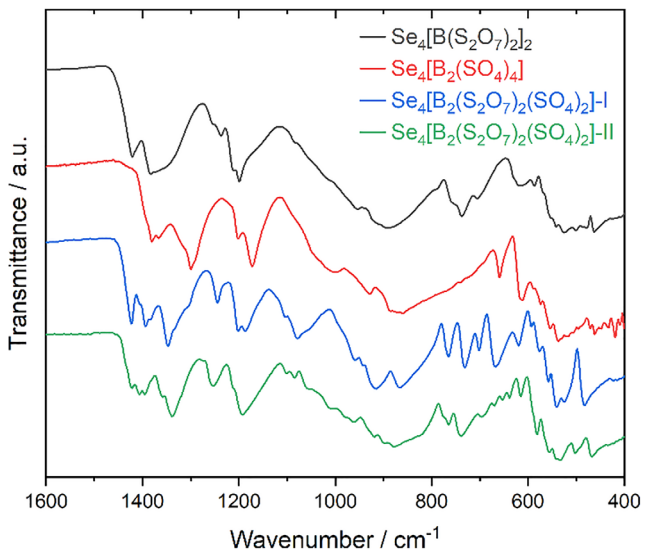


FIGURE 11 | Infrared spectra of $Se_4[B(S_2O_7)_2]_2$ (black), $Se_4[B_2(SO_4)_4]$ (red), $Se_4[B_2(SO_4)_2(S_2O_7)_2]$-I (blue), and $Se_4[B_2(SO_4)_2(S_2O_7)_2]$-II (green) between 1600 and 400 cm^{-1}.

strength. The additional broad band around 700 nm presumably originates from transitions within Se_8^{2+} ions occasionally formed from unreacted Se_4^{2+} ions yielding a greenish hue – which happens if the sample gets into contact with reducing agents [18]. Essentially, this suggests that we might see a borosulfate featuring Se_8^{2+} soon.

2.10 | Infrared Spectroscopy

In Figure 11, the infrared spectra of $Se_4[B(S_2O_7)_2]_2$, $Se_4[B_2(SO_4)_2(S_2O_7)_2]$-I, $Se_4[B_2(SO_4)_2(S_2O_7)_2]$-II, and $Se_4[B_2(SO_4)_4]$ between 1500 and 400 cm^{-1} are displayed — full spectra are shown in Figure S4 — and reveal bands typical for borate and sulfate tetrahedra. The assignments in the

15213773, 2026, 45, Downloaded from https://onlinelibrary.wiley.com/doi/10.1002/anie.430417 by Universitätsbibliothek Augsburg, Wiley Online Library on [08/11/2026]. See the Terms and Conditions (https://onlinelibrary.wiley.com/terms-and-conditions) on Wiley Online Library for rules of use; OA articles are governed by the applicable Creative Commons License

TABLE 3 | Diffuse reflectance spectra and electronic absorption of Se_4^{2+} in various compounds reported previously compared to $Se_4[B(S_2O_7)_2]_2$

Species	Color	$\pi \rightarrow \pi^*$ transition $2b_g/1b_g \rightarrow 2a_u$	$\pi \rightarrow \pi^*$ transition $2b_g/1b_g \rightarrow 5b_u/6b_u$	References
Se_4^{2+} (solution)	yellow	410	320	[20]
$Se_4[Sb_2F_4][Sb_2F_5][SbF_6]_5$	yellow	413	382	[60]
$Se_4[AsF_6]_2$	yellow	440	385	[60]
$Se_4[B(S_2O_7)_2]_2$	yellow	444	392	this work
$Se_4[AlCl_4]_2$	orange	488	430	[60]
$Se_4[HS_2O_7]_2$	orange	524	428	[60]

recorded spectra were achieved by comparing the bands to experimental and calculated data of $Ba[B(S_2O_7)_2]$, a borosulfate that also features S–O–S bridges and even contains the same $[B(S_2O_7)_2]^{2-}$ anion [48]. Above 1500 cm^{-1}, two broad bands centred around 2930 and 2425 cm^{-1} occur and can be assigned to small amounts of adhesive sulfuric acid [70]. The bands between 1430 and 1330 cm^{-1} can be assigned to asymmetric stretching vibrations ν_{as}(S–O). Symmetric stretching vibrations ν_s(S–O_t) of terminal oxygen atoms are found between 1215 and 1185 cm^{-1}. In the region from 1105 to 940 cm^{-1}, symmetric and asymmetric stretching vibrations $\nu_{s/as}$(B–O) in (BO_4) tetrahedra occur. Bending vibrations δ(O–B–O) are found in the region 920–870 cm^{-1}. The bands between 770 and 640 cm^{-1} can be assigned to stretching vibrations ν_s(S–O_b) of bridging oxygen atoms within the (S_2O_7) groups, confirming the presence of S–O–S bridges. Lastly, between 615 and 460 cm^{-1}, bending vibrations of the (BO_4) δ(O–B–O) and (SO_4) tetrahedra δ(O–S–O) can be found. Due to the limited range of the spectrometer, Se–Se vibrations could not be further evaluated. These bands are typically found around 320 cm^{-1} [60].

2.11 | Thermal Analysis

The transformation of borosulfates into other borosulfates is well known. Compounds comprising S–O–S bridges typically decompose towards compounds containing B–O–S bridges and finally B–O–B bridges as observed in the series of the barium borosulfates $Ba[B(S_2O_7)_2]_2$, $Ba[B_2(SO_4)_4]$, and $Ba[B_2O(SO_4)_3]$ [48]. However, it is important to note that these transformations do not occur in all cases, but they can depend on the environment during the decomposition process; for instance, under nitrogen atmosphere, the decomposition of $Sr[B_2(SO_4)_4]$ immediately leads to the formation of $SrSO_4$ while in mother liquor the formation of $Sr[B_2O(SO_4)_3]$ is observed [53]. Similarly, during the decomposition of $Sr[B_2(SO_4)_3(S_2O_7)]$ in a capillary, monitored by X-ray diffraction analysis, $Sr[B_2O(SO_4)_3]$ was verified as an intermediate [71]. Hence, high sulfate or SO_3 concentrations in a closed environment during decomposition foster the formation of further borosulfates.

A powerful tool to identify the composition of crystalline products with increasing temperature is the temperature-programmed powder X-ray diffraction (TPPXRD). These experiments were carried out in a capillary and revealed a structural relationship between all five borosulfates of this work. The diffraction patterns in Figure 12a indicate a thermal stability of $Se_4[B(S_2O_7)_2]_2$ until 80°C. At 100°C, with the release of two moles SO_3 the *bis*-disulfatoborat groups condense to form larger zero-dimensional anions, still featuring S–O–S bridges:

$$Se_4[B(S_2O_7)_2]_2 \rightarrow Se_4[B_2(SO_4)_2(S_2O_7)_2]\text{-I} + 2SO_{3(g)} \quad (1)$$

Subsequently, $Se_4[B_2(SO_4)_2(S_2O_7)_2]$-I decomposes at 150°C to form $Se_4[B_2(SO_4)_4]$, a one-dimensional borosulfate comprising B–O–S bridges. Hence, this compound is stable up to 200°C:

$$Se_4[B_2(SO_4)_2(S_2O_7)_2]\text{-I} \rightarrow Se_4[B_2(SO_4)_4] + 2SO_{3(g)} \quad (2)$$

In comparison, Figure 13c shows the decomposition process starting from the related selenium *bis*-borodisulfate $Se_4[B(S_2O_7)_2]_2(SO_3)$ still containing molecular SO_3 units. In a first step, at 80°C the incorporated molecular SO_3 is evaporated to transform into the SO_3-free analogue:

$$Se_4[B(S_2O_7)_2]_2(SO_3) \rightarrow Se_4[B(S_2O_7)_2]_2 + SO_{3(g)} \quad (3)$$

Like in the earlier discussed case, $Se_4[B(S_2O_7)_2]_2$ decomposition starts at 100°C, however, now to form polymorph II of $Se_4[B_2(SO_4)_2(S_2O_7)_2]$. This time, the $[B(S_2O_7)_2]^{2-}$ units condense to form chains:

$$Se_4[B(S_2O_7)_2]_2 \rightarrow Se_4[B_2(SO_4)_2(S_2O_7)_2]\text{-II} + 2SO_{3(g)} \quad (4)$$

$Se_4[B_2(SO_4)_2(S_2O_7)_2]$-II starts to decompose around 125°C. Minor reflections can be assigned to $Se_4[B_2(SO_4)_4]$ and indicate a lower thermal stability compared to the first polymorph which is in accordance with the general trend observed within borosulfates where the thermal stability decreases with increasing dimensionality [72]:

$$Se_4[B_2(SO_4)_2(S_2O_7)_2]\text{-II} \rightarrow Se_4[B_2(SO_4)_4] + 2SO_{3(g)} \quad (5)$$

Finally, $Se_4[B_2(SO_4)_4]$ decomposes above 200°C to form an amorphous residue consistent with the first TPPXRD experiment. It seems that different SO_3 partial pressures in the closed system allow for two alternative decomposition processes. Both differ only regarding an additional SO_3 unit per sum formula of the starting material. This transformation from one compound to another, where both contain S–O–S bridges, is a unique feature of this system which was observed for the first time in borosulfate chemistry.

15213773, 2026, 45, Downloaded from https://onlinelibrary.wiley.com/doi/10.1002/anie.430417 by Universitatsbibliothek Augsburg, Wiley Online Library on [08/11/2026]. See the Terms and Conditions (https://onlinelibrary.wiley.com/terms-and-conditions) on Wiley Online Library for rules of use; OA articles are governed by the applicable Creative Commons License

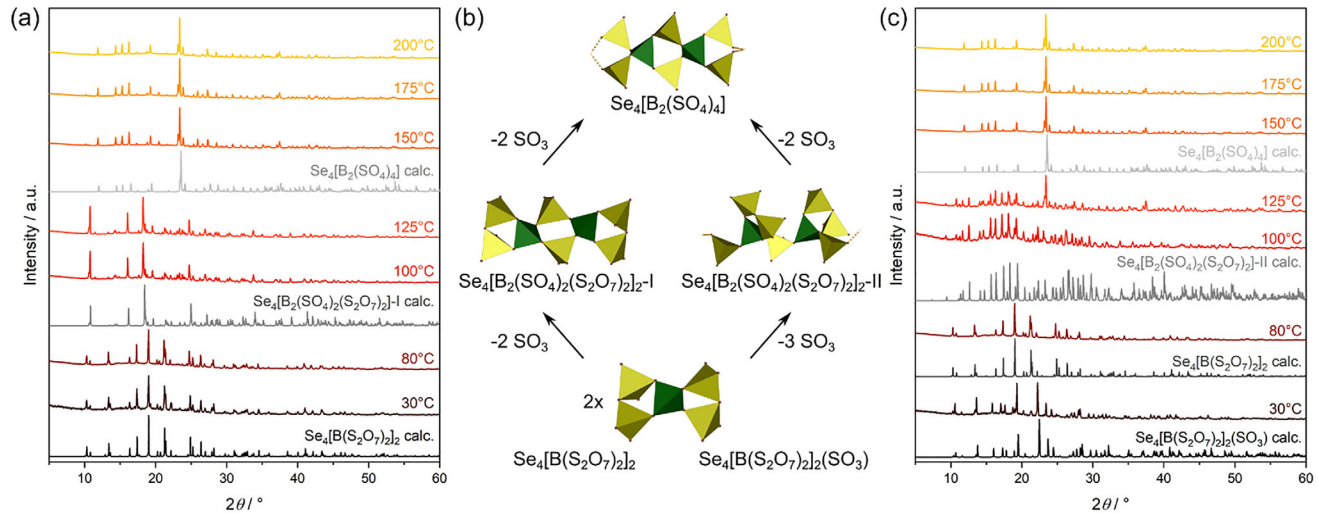


FIGURE 12 | TPPXRD patterns of (a) $Se_4[B(S_2O_7)_2]_2$ and c) $Se_4[B(S_2O_7)_2]_2(SO_3)$. (b) Schematic representation of the stepwise condensation from the $[B(S_2O_7)_2]^-$ anion in $Se_4[B(S_2O_7)_2]_2$ and $Se_4[B(S_2O_7)_2]_2(SO_3)$ dependent on the SO_3 content within the capillary over the zero- and one-dimensional anions $[B_2(SO_4)_2(S_2O_7)_2]^-$ of the two polymorphs in $Se_4[B_2(SO_4)_2(S_2O_7)_2]$ to the final decomposition product $Se_4[B_2(SO_4)_4]$ with the $[B_2(SO_4)_4]^-$ anion by the release of further two moles of SO_3.

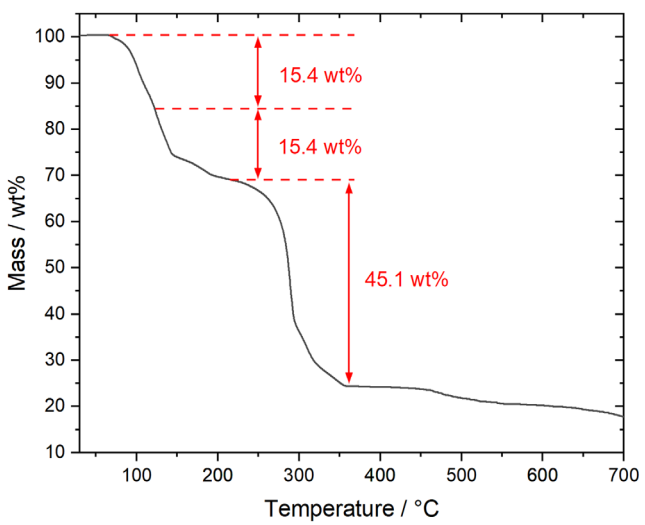


FIGURE 13 | Thermal analysis of $Se_4[B(S_2O_7)_2]_2$ in a nitrogen atmosphere with a heating rate of 5 K·min^{-1}.

To verify the results of the TPPXRD experiments, we further employed thermogravimetric analyses (TGA) (Figure 13). Due to the volatility of SO_3 in $Se_4[B(S_2O_7)_2]_2(SO_3)$, already evaporating at room temperature over time, a conclusive measurement was not possible. Considering the SO_3-free compound, the mass losses from Equations (1) and (2) of 14.9 % and 15.6 % agree well with the evaporation of two moles SO_3 per step (Δm_{calc} = 15.4%) and the formation of $Se_4[B_2(SO_4)_4]$. The intermediate formation of one of the polymorphs overlays with its decomposition caused by the small stability regime leading to no proper development of a plateau. The residue after the decomposition of $Se_4[B_2(SO_4)_4]$ was not unambiguously determined as the powder was amorphous. Nevertheless, the red body color hints to the formation of red selenium which is typical to be formed at these temperatures; this agrees with the PXRD results (Equation (5)).

3 | Conclusion

The stabilization of polycations of group 16 elements in the solid state almost exclusively occurs in Lewis acidic (transition) metal (oxo)halides that provide weakly coordinating anions, a precondition for their stabilization. In this contribution, we report on six compounds stabilising the Se_4^{2+} cation in a Brønsted acidic, purely oxoanionic coordination environment representing a significant contribution towards the stabilization of these compounds since $Se_4[HS_2O_7]_2$ was synthesized in 1968.

Herein, we added the first five borosulfates hosting Se_4^{2+} ions. Both $Se_4[B(S_2O_7)_2]_2(SO_3)$ and $Se_4[B(S_2O_7)_2]_2$ feature the well-known $[B(S_2O_7)_2]^-$ anion; the former can be converted into the latter by evaporation of the volatile SO_3. $Se_4[B_2(SO_4)_2(S_2O_7)_2]$ forms two polymorphs with rare zero- and one-dimensional anions. Finally, we synthesised $Se_4[B_2(SO_4)_4]$, a borosulfate comprising well-known SiS_2-like chains, substituting B by Si and (SO_4) by S. In this study, we also solved the crystal structure of $Se_4[S_4O_{13}]$, a compound discovered in 1968 but not structurally characterized to date. The compound exhibits the uncommon tetrasulfate anion.

It is well known that the color of compounds containing Se_4^{2+} cations red shifts from yellow to red with increasing coordination strength of the anion. Accordingly, the yellow color observed for all five borosulfates and the tetrasulfate confirms the weak coordination of borosulfates and polysulfates. Therefore, we recorded the very first powder reflectance spectra of solids containing Se_4^{2+} and observed, among others, a strong absorption in the blue regime responsible for the compound's color. Based on LOBSTER calculations this band can be attributed to $\pi^* \leftarrow \pi$ transitions within the selenium ring. This transition energy depends on the coordination strength of the chemical surrounding and confirms the relation between color and coordination strength. LOBSTER also provided insights into the bonding situation and charge distribution in Se_4^{2+}. These results are in excellent accordance with

15213773, 2026, 45, Downloaded from https://onlinelibrary.wiley.com/doi/10.1002/anie.430417 by Universitatsbibliothek Augsburg, Wiley Online Library on [08/11/2026]. See the Terms and Conditions (https://onlinelibrary.wiley.com/terms-and-conditions) on Wiley Online Library for rules of use; OA articles are governed by the applicable Creative Commons License

magnetic measurements on $Se_4[B(S_2O_7)_2]_2(SO_3)$ and $Se_4[S_4O_{13}]$, confirming their diamagnetism, hence, the absence of unpaired electrons in the selenium cation.

Moreover, TPPXRD measurements reveal that the borosulfates of this study form sequentially with increasing decomposition temperature, enabling their selective synthesis. For the first time in borosulfates, the loss of an SO_3 entity could be directly tracked. The borosulfates $Se_4[B(S_2O_7)_2]_2(SO_3)$ and $Se_4[B(S_2O_7)_2]_2$, differing only by the presence of one SO_3 molecule decompose to the common intermediate phase, $Se_4[B_2(SO_4)_2(S_2O_7)_2]$, which was observed in two distinct modifications. These modifications can be selectively obtained depending on whether the SO_3-containing or SO_3-free precursor is thermally decomposed. The further decomposition yields the same phase, that is $Se_4[B_2(SO_4)_4]$. This colorful and diverse chemistry suggests that there is a lot more to come regarding compounds containing group 16 oligocations.

Author Contributions

Erich Turgunbajew: conceptualization, methodology, data curation, writing – review and editing, writing – original draft, visualization, validation, investigation, project administration. **Marios Symeonidis**: investigation, visualization, writing – review and editing. **Jörn Bruns**: writing – review and editing, visualization, validation, investigation, project administration, supervision, resources, writing – original draft. **Sara N. Özbay**: writing – review and editing, investigation. **Jan Langwald**: investigation, visualization, writing – review and editing. **Mathias S. Wickleder**: writing – review and editing, visualization, validation, resources, writing – original draft. **Robert E. Dinnebier**: investigation, writing – review and editing, visualization, resources. **Linda S. Reitz**: visualization, writing – review and editing, investigation. **Richard Dronskowski**: investigation, writing – review and editing, software, visualization, validation, resources, writing – original draft. **Lars Schumacher**: visualization, investigation, writing – review and editing. **Rainer Pöttgen**: writing – review and editing, data curation, funding acquisition, visualization, validation, resources, writing – original draft. **Henning A. Höppe**: conceptualization, validation, funding acquisition, project administration, writing – original draft, writing – review and editing, supervision, data curation, formal analysis, resources.

Acknowledgments

E. T. and H. A. H. thank the Deutsche Forschungsgemeinschaft (DFG) for financial support under the project no. 556118528. This research was funded by Universität Münster and Deutsche Forschungsgemeinschaft (INST 211/1034-1). J. L. is thankful to the German National Scholarship Foundation (Studienstiftung des Deutschen Volkes) for financial support.

Open access funding enabled and organized by Projekt DEAL.

Conflicts of Interest

The authors declare no conflicts of interest.

Data Availability Statement

The data that support the findings of this study are available from the corresponding author upon reasonable request.

References

1. F. J. Müller von Reichenstein, "Versuche mit dem in der Grube Maria Hilf in dem Gebirge Faczebai bei Zalathna in Siebenbürgen vorkommenden vermeinten gediegenen Spiesglaskönige," *Physikalische Arbeiten der einträchtigen Freunde in Wien* 1 (1784): 49–53.

2. M. H. Klaproth, "XVIII. Extract From a Memoir on a new Metal Called Tellurium," *Philosophical Magazine* 1 (1798): 78–82, https://doi.org/10.1080/14786447808676799.

3. C. F. Buchholz, "Versuche über die Auflösung des Indigs in der Schwefelsäure, als Beitrag zur Ausmittelung des Vorgangs ein derselben," *Gehlen´s neues Journal of Chemistry* 3 (1804): 7.

4. J. J. Berzelius, "Ueber das Selenium," *Schweigger´s Journal of Chemical Physics* 21 (1817): 342.

5. J. J. Berzelius, "Untersuchung eines neuen, in den unreinen Arten des zu Fahlun bereiteten Schwefels gefundenen Mineral-Körpers. Über das Selenium," *Schweigger´s Journal of Chemical Physics* 23 (1818): 308–344.

6. E. Divers and M. Shimosé, "XL.- On a New Oxide of Tellurium," *Journal of the Chemical Society, Transactions* 43 (1883): 319–323.

7. E. Divers and M. Shimosé, "XLI.- On Tellurium Sulphoxide," *Journal of the Chemical Society, Transactions* 43 (1883): 323–329.

8. E. Divers and M. Shimosé, "XLII.- On a New Reaction of Tellurium Compounds," *Journal of the Chemical Society, Transactions* 43 (1883): 329–331.

9. I. Vogel and J. R. Partington, "CCII. – Sulphur Sesquioxide," *Journal of the Chemical Society, Transactions* 127 (1925): 1514–1524.

10. R. Weber, "Ueber eine neue Sauerstoffverbindung des Schwefels und ein derselben analoges Selensubstitutionsprodukt," *Annals of Physics (Leipzig)* 12 (1875): 531–553.

11. H. Lux and E. Böhm, "Über die blauen Lösungen des Schwefels, II. Lösungen des Schwefels in Oleum," *Chemische Berichte* 98 (1965): 3210–3217, https://doi.org/10.1002/cber.19650981018.

12. J. Arotsky and M. C. R. Symons, "Ionic Conductivity in Concentrated Oleums," *Transactions of the Faraday Society* 56 (1960): 1426–1431.

13. G. Magnus, "Ueber die Eigenschaft der Schwefelsäure, oxydirbare einfache Körper aufzulösen ohne dieselben zu oxydiren," *Annals of Physics (Leipzig)* 87 (1827): 491–494.

14. G. Magnus, "Bemerkung über die Auflösung des Selens in Schwefelsäure," *Annals of Physics (Leipzig)* 10 (1828): 328.

15. N. W. Fischer, "Ob das Tellur metallisch in concentrirter Schwefelsäure gelöst enthalten seyn könne," *Annals of Physics (Leipzig)* 87 (1828): 153–155.

16. N. W. Fischer, "Ueber die Natur der rothen Auflösung des Tellurs in Schwefelsäure, als Fortsetzung der in diesen Annalen, Bd. 12. S. 158., mitgetheilten Notiz," *Annals of Physics (Leipzig)* 91 (1829): 77–81.

17. N. W. Fischer, "Zusatz zu meiner Notiz über die Auflösung des Tellurs in Schwefelsäure," *Annals of Physics (Leipzig)* 92 (1829): 118–124, https://doi.org/10.1002/andp.18290920511.

18. J. Barr, R. J. Gillespie, R. Kapoor, and K. C. Malhotra, "New Polyatomic Cations of the Group VI B Elements: I. Solutions of Selenium in Highly Acidic Solvents," *Canadian Journal of Chemistry* 46 (1968): 149–159.

19. N. J. Bjerrum and G. P. Smith, "Tellurium in the Formal Electropositive Oxidation state One-half in Acidic Chloride media," *Journal of the American Chemical Society* 90 (1968): 4472–4473.

20. J. Barr, D. B. Crump, R. J. Gillespie, R. Kapoor, and P. K. Ummat, "Polyatomic Cations of the Group VIB Elements. II. Compounds of the Se_4^{2+} Cation," *Canadian Journal of Chemistry* 46 (1968): 3607–3609.

21. I. D. Brown, D. B. Crump, R. J. Gillespie, and D. P. Santry, "The Structure of the Se_4^{2+} Ion," *Journal of the Chemical Society D: Chemical Communications* 4 (1968): 853–854.

22. I. D. Brown, D. B. Crump, and R. J. Gillespie, "Crystal Structure of Tetraselenium Bis(hydrogen disulfate)," *Inorganic Chemistry* 10 (1971): 2319–2323.

23. D. J. Prince, J. D. Corbett, and B. Garbisch, "Polyatomic Cations of Tellurium and Selenium in Chloroaluminate Salts. A Study of the Systems M-(MCl_4 + $4AlCl_3$)," *Inorganic Chemistry* 9 (1970): 2731–2735.

15213773, 2026, 45, Downloaded from https://onlinelibrary.wiley.com/doi/10.1002/anie.430047 by Universitätsbibliothek Augsburg, Wiley Online Library on [08/11/2026]. See the Terms and Conditions (https://onlinelibrary.wiley.com/terms-and-conditions) on Wiley Online Library for rules of use; OA articles are governed by the applicable Creative Commons License

24. R. J. Gillespie, J. Passmore, P. K. Ummat, and O. C. Vaidya, "Polyatomic Cations of Sulfur. I. Preparation and Properties of S_{16}^{2+}, S_8^{2+}, and S_4^{2+}," *Inorganic Chemistry* 10 (1971): 1327–1332.

25. J. Beck, "New Forms and Functions of Tellurium: From Polycations to Metal Halide Tellurides," *Angewandte Chemie International Edition* 33 (1994): 163–172, https://doi.org/10.1002/anie.199401631.

26. J. Beck, "Rings, Cages and Chains—the Rich Structural Chemistry of the Polycations of the Chalcogens," *Coordination Chemistry Reviews* 163 (1997): 55–70.

27. J. Beck and G. Bock, "Te_8^{4+}: A Cubic Polycation in the Structure of $Te_8(VOCl_4)_2$," *Angewandte Chemie International Edition* 34 (1995): 2559–2561, https://doi.org/10.1002/anie.199525591.

28. S. Schlüter, *Dissertation* (Rheinische Friedrich-Wilhelms-Universität Bonn, 2004).

29. S. Brownridge, "Recent Advances in the Understanding of the Syntheses, Structures, Bonding and Energetics of the Homopolyatomic Cations of Groups 16 and 17," *Coordination Chemistry Reviews* 197 (2000): 397–481.

30. E. Ahmed and M. Ruck, "Homo- and Heteroatomic Polycations of Groups 15 and 16. Recent Advances in Synthesis and Isolation Using Room Temperature Ionic Liquids," *Coordination Chemistry Reviews* 255 (2011): 2892–2903, https://doi.org/10.1016/j.ccr.2011.06.011.

31. J. Langwald, S. Burguera, A. Frontera, and M. S. Wickleder, "Structural Insights Into Heavy Chalcogen Polycations and Their Stabilization via (hydrogen)Polysulfates," *Dalton Transactions* 55 (2026): 9485–9495, https://doi.org/10.1039/d6dt01115b.

32. R. J. Gillespie, T. E. Peel, and E. A. Robinson, "Hammett Acidity Function for some Super Acid Systems. I. Systems H_2SO_4-SO_3, H_2SO_4-HSO_3F, H_2SO_4-HSO_3Cl, and H_2SO_4-$HB(HSO_4)_4$," *Journal of the American Chemical Society* 93 (1971): 5083–5087.

33. H. A. Höppe, K. Kazmierczak, M. Daub, K. Förg, F. Fuchs, and H. Hillebrecht, "The First Borosulfate $K_5[B(SO_4)_4]$," *Angewandte Chemie International Edition* 51 (2012): 6255–6257, https://doi.org/10.1002/anie.201109237.

34. M. Daub, H. A. Höppe, and H. Hillebrecht, "Further New Borosulfates: Synthesis, Crystal Structure, and Vibrational Spectra of $A[B(SO_4)_2]$ (A = Na, K, NH_4) and the Crystal Structures of $Li_5[B(SO_4)_4]$ and $NH_4[B(S_2O_7)_2]$," *Zeitschrift für anorganische und allgemeine Chemie* 640 (2014): 2914–2921, https://doi.org/10.1002/zaac.201400315.

35. J. Bruns, M. Podewitz, M. Schauperl, et al., "$Ag[B(SO_4)_2]$—Synthesis, Crystal Structure, and Characterization of the First Precious-Metal Borosulfate," *European Journal of Inorganic Chemistry* 2017 (2017): 3981–3989, https://doi.org/10.1002/ejic.201700360.

36. M. Hämmer, L. C. Pasqualini, S. S. Sebastian, H. Huppertz, H. A. Höppe, and J. Bruns, "$Cd[B_2(SO_4)_4]$ and $H_2[B_2(SO_4)_4]$—a Phyllosilicate-analogous Borosulfate and Its Homeotypic Heteropolyacid," *Dalton Transactions* 51 (2022): 15458–15466, https://doi.org/10.1039/d2dt02344j.

37. M. Daub, K. Kazmierczak, P. Gross, H. Höppe, and H. Hillebrecht, "Exploring a New Structure family: Alkali Borosulfates $Na_5[B(SO_4)_4]$, $A_3[B(SO_4)_3]$ (A = K, Rb), $Li[B(SO_4)_2]$, and $Li[B(S_2O_7)_2]$," *Inorganic Chemistry* 52 (2013): 6011–6020, https://doi.org/10.1021/ic400267s.

38. P. Netzsch, F. Pielnhofer, R. Glaum, and H. A. Höppe, "Synthesis-Controlled Polymorphism and Optical Properties of Phyllosilicate-Analogous Borosulfates $M[B_2(SO_4)_4]$ (M = Mg, Co)," *Chemistry: A European Journal* 26 (2020): 14745–14753, https://doi.org/10.1002/chem.202003214.

39. P. Netzsch, M. Hämmer, P. Gross, et al., "$RE_2[B_2(SO_4)_6]$ (RE = Y, La-Nd, Sm, Eu, Tb-Lu): A Silicate-analogous Host Structure With Weak Coordination Behaviour," *Dalton Transactions* 48 (2019): 4387–4397, https://doi.org/10.1039/c9dt00445a.

40. E. Turgunbajew, G. Buchner, A. Koldemir, et al., "Mössbauer Spectroscopy on Antimony Borosulfates Reveals Weak Coordination Behavior," *Angewandte Chemie International Edition* 65 (2026): e21198, https://doi.org/10.1002/anie.202521198.

41. D. van Gerven, S. Sutorius, J. Bruns, and M. S. Wickleder, "Stabilizing the Homopolycation $(I_4)^{2+}$ With a Hexasulfate in $(I_4)[S_6O_{19}]$ and a Borosulfate in $(I_4)[B(S_2O_7)_2]_2$," *ChemistryOpen* 11 (2022): e202200122.

42. L. V. Schindler, A. Becker, M. Wieckhusen, T. Klüner, and M. S. Wickleder, "Polysulfates $[SnO_{3n+1}]^{2-}$: With the $[S_6O_{19}]^{2-}$ Anion, Has the End Been Reached?," *Angewandte Chemie International Edition* 55 (2016): 16165–16167, https://doi.org/10.1002/anie.201607629.

43. C. Logemann, T. Klüner, and M. S. Wickleder, "The Elusive Tetrasulfate Anion $[S_4O_{13}]^{2-}$," *Angewandte Chemie International Edition* 51 (2012): 4997–5000, https://doi.org/10.1002/anie.201108206.

44. J. Langwald, R. M. Gomila, D. van Gerven, A. Frontera, and M. S. Wickleder, "Introducing (inter-)Halogen Polysulfates—a Study on the Influence of Halogen Bonding on Weakly Coordinating Anions," *Dalton Transactions* 54 (2025): 16095–16105, https://doi.org/10.1039/d5dt02088c.

45. L. V. Schindler, A. Becker, and M. S. Wickleder, "Stabilizing Superacid Anions: The New $[H(S_4O_{13})_2]^{3-}$ Anion in the Crystal Structure of $Li_3[H(S_4O_{13})_2]$," *Chemistry: A European Journal* 22 (2016): 17538–17541, https://doi.org/10.1002/chem.201603919.

46. M. Daub, K. Kazmierczak, H. A. Höppe, and H. Hillebrecht, "The Borosulfate Story Goes On-From Alkali and Oxonium Salts to Polyacids," *Chemistry: A European Journal* 19 (2013): 16954–16962, https://doi.org/10.1002/chem.201303012.

47. P. Netzsch and H. A. Höppe, "$Ag[B(S_2O_7)_2]$: The First Transition Metal Borosulfate Featuring Disulfate Groups," *European Journal of Inorganic Chemistry* 2021 (2021): 1065–1070, https://doi.org/10.1002/ejic.202001095.

48. P. Netzsch, F. Pielnhofer, and H. A. Höppe, "From S-O-S to B-O-S to B-O-B Bridges: $Ba[B(S_2O_7)_2]_2$ as a Model System for the Structural Diversity in Borosulfate Chemistry," *Inorganic Chemistry* 59 (2020): 15180–15188, https://doi.org/10.1021/acs.inorgchem.0c02156.

49. S. Sutorius, D. van Gerven, S. Olthof, B. Rasche, and J. Bruns, "Polycations Stabilised by Borosulfates: $[Au_3Cl_4][B(S_2O_7)_2]$ and the One-Dimensional Metal $[Au_2Cl_4][B(S_2O_7)_2](SO_3)$," *Chemistry: A European Journal* 28 (2022): e202200004, https://doi.org/10.1002/chem.202200004.

50. F. Liebau, *Structural Chemistry of Silicates. Structure, Bonding, and Classification* (Springer Heidelberg, 1985).

51. S. Sutorius, D. Patrun, A. Edelmann, et al., "$Pd[B(S_2O_7)_2]_2$ and $Pd[B(SO_4)(S_2O_7)]_2$: Two Borosulfates With Pd^{2+} in Octahedral and One With Pd^{2+} in Square Planar Oxygen Coordination," *Chemistry: A European Journal* 31 (2025): e202501515, https://doi.org/10.1002/chem.202501515.

52. S. Schönegger, J. Bruns, B. Gartner, K. Wurst, and H. Huppertz, "Synthesis and Characterization of the First Lead(II) Borosulfate $Pb[B_2(SO_4)_4]$," *Zeitschrift für anorganische und allgemeine Chemie* 644 (2018): 1702–1706, https://doi.org/10.1002/zaac.201800130.

53. P. Netzsch and H. A. Höppe, "Synthesis and Characterization of the Chain Borosulfates $(NH_4)_3[B(SO_4)_3]$ and $Sr[B_2(SO_4)_4]$," *Zeitschrift für anorgische und allgemeine Chem* 646 (2020): 1563–1569, https://doi.org/10.1002/zaac.202000105.

54. R. Hübenthal, *MAPLE: Programm for Calculation of the Madelung Part of Lattice Energy* (Universität Gießen, 1993).

55. R. Hoppe, "Madelung Constants," *Angewandte Chemie International Edition* 5 (1966): 95–106, https://doi.org/10.1002/anie.196600951.

56. R. Hoppe, "Über Madelungfaktoren," *Angewandte Chemie* 78 (1966): 52–63, https://doi.org/10.1002/ange.19660780106.

57. R. Hoppe, "The Coordination Number – an Inorganic Chameleon," *Angewandte Chemie International Edition* 9 (1970): 25–34, https://doi.org/10.1002/anie.197000251.

58. R. Hoppe, "Effective Coordination Numbers (ECoN) and Mean Fictive Ionic Radii (MEFIR)," *Zeitschrift für Kristallographie* 150 (1979): 23–52.

59. R. C. Burns, R. J. Gillespie, J. A. Barnes, and M. J. McGlinchey, "Molecular Orbital Investigation of the Structure of some Polyatomic

15213773, 2026, 45, Downloaded from https://onlinelibrary.wiley.com/doi/10.1002/anie.430417 by Universitätsbibliothek Augsburg, Wiley Online Library on [08/11/2026]. See the Terms and Conditions (https://onlinelibrary.wiley.com/terms-and-conditions) on Wiley Online Library for rules of use; OA articles are governed by the applicable Creative Commons License

Cations and Anions of the Main-group Elements," *Inorganic Chemistry* 21 (1982): 799–807.

60. R. C. Burns and R. J. Gillespie, "Vibrational Spectra and Analyses of the S_4^{2+}, Se_4^{2+}, Te_4^{2+}, and *Trans*-$Te_2Se_2^{2+}$ Polyatomic Cations," *Inorganic Chemistry* 21 (1982): 3877–3886.

61. G. Cardinal, R. J. Gillespie, J. F. Sawyer, and J. E. Vekris, "Charge-transfer Interactions in the Square-planar Chalcogen Cations, M_4^{2+}: Preparation and Crystal Structures of the Compounds $(Se_4^{2+})(Sb_2F_4^{2+})(Sb_2F_5^{+})(SbF_6^{-})_5$, $(Se_4^{2+})(AlCl_4^{-})_2$, and $(Te_4^{2+})(SbF_6^{-})_2$,"*Journal of the Chemical Society, Dalton Transactions* 11 (1982): 765–779.

62. R. Minkwitz, H. Borrmann, and J. Nowicki, "Darstellung und Kristallstruktur von $(Se_4)_2(Sb_4F_{17})(SbF_6)_3$ /Preparation and Crystal Structure of $(Se_4)_2(Sb_4F_{17})(SbF_6)_3$," *Zeitschrift für Naturforschung Teil B Chemie, Biochemie, Biophysik Biologie und verwandte Gebiete* 46 (1991): 629–634.

63. J. Beck and F. Steden, "$[Bi_6F_{11}]^{7+}$—an Unusual, Highly Charged Bismuth Fluoro Complex in $(Se_4)[Bi_6F_{11}][AsF_6]_9 \cdot 10\ SO_2$," *Chemical Communications* 41 (2005): 5453–5455, https://doi.org/10.1039/b508898d.

64. J. Beck and K. Schlitt, "Chalcogen Polycations With Mononuclear Divalent Anions From Chalcogen Subhalides and Tetrachlorides of Zr and Hf: Syntheses and Crystal Structures of $Se_4(MCl_6)$ (M = Zr, Hf) and $Te_4(HfCl_6)$," *Chemische Berichte* 128 (1995): 763–766, https://doi.org/10.1002/cber.19951280804.

65. J. Beck and T. Hilbert, "Selen-Polykationen stabilisiert durch polymere Chlorobismutat-Anionen: Synthesen und Kristallstrukturen von $Se_4[Bi_4Cl_{14}]$ und $Se_{10}[Bi_5Cl_{17}]$," *Zeitschrift für anorganische und allgemeine Chemie* 626 (2000): 837–844, https://doi.org/10.1002/(SICI)1521-3749(200004)626:4⟨837::AID-ZAAC837⟩3.0.CO;2-J.

66. P. C. Müller, L. S. Reitz, D. Hemker, and R. Dronskowski, "Orbital-based Bonding Analysis in Solids," *Chemical Science* 16 (2025): 12212–12226, https://doi.org/10.1039/d5sc02936h.

67. P. C. Müller, C. Ertural, J. Hempelmann, and R. Dronskowski, "Crystal Orbital Bond Index: Covalent Bond Orders in Solids," *Journal of Physical Chemistry C* 125 (2021): 7959–7970, https://doi.org/10.1021/acs.jpcc.1c00718.

68. P. C. Müller, N. Schmit, L. Sann, S. Steinberg, and R. Dronskowski, "Fragment Orbitals Extracted From First-Principles Plane-Wave Calculations," *Inorganic Chemistry* 63 (2024): 20161–20172, https://doi.org/10.1021/acs.inorgchem.4c01024.

69. G. A. Bain and J. F. Berry, "Diamagnetic Corrections and Pascal's Constants," *Journal of Chemical Education* 85 (2008): 532–536.

70. A. B. Horn and K. Jessica Sully, "ATR-IR Spectroscopic Studies of the Formation of Sulfuric Acid and Sulfuric Acid Monohydrate Films," *Physical Chemistry Chemical Physics* 1 (1999): 3801–3806.

71. P. Netzsch and H. A. Höppe, "$SrB_2(SO_4)_3(S_2O_7)$: A Borosulfate With an Unprecedented Chain Structure Comprising Disulfate Groups," *Inorganic Chemistry* 59 (2020): 18102–18108, https://doi.org/10.1021/acs.inorgchem.0c02560.

72. E. Turgunbajew, M. Hämmer, L. Bayarjargal, F. Pielnhofer, and H. A. Höppe, "Variability of a Non-Centrosymmetric Tecto-Borosulfate: Introduction of Various Molecular Cations Into $BiX[B(SO_4)_2]_4$ (X = H_3O^+, NO_2^+, NH_4^+, NO^+)," *Chemistry: A European Journal* 31 (2025): e02439, https://doi.org/10.1002/chem.202502439.

73. Bruker *SADABS* (Bruker AXS Inc., 2012).

74. G. M. Sheldrick, "A Short History of SHELX," *Acta Crystallographica Section A, Crystal Physics, Diffraction, Theoretical and General Crystallography* 64 (2008): 112–122, https://doi.org/10.1107/S0108767307043930.

75. G. M. Sheldrick, "Crystal Structure Refinement With SHELXL," *Acta Crystallographica Section C, Crystal Structure Communications* 71 (2015): 3–8, https://doi.org/10.1107/S2053229614024218.

76. A. A. Coelho, "TOPAS and TOPAS-Academic: An Optimization Program Integrating Computer Algebra and Crystallographic Objects Written in C++," *Journal of Applied Crystallography* 51 (2018): 210–218, https://doi.org/10.1107/S1600576718000183.

77. P. Thompson, D. E. Cox, and J. B. Hastings, "Rietveld Refinement of Debye-Scherrer Synchrotron X-ray Data From Al_2O_3," *Journal of Applied Crystallography* 20 (1987): 79–83.

78. A. A. Coelho, "Indexing of Powder Diffraction Patterns by Iterative Use of Singular Value Decomposition," *Journal of Applied Crystallography* 36 (2003): 86–95.

79. G. S. Pawley, "Unit-Cell Refinement from Powder Diffraction Scans," *Journal of Applied Crystallography* 14 (1981): 357–361.

80. R. W. Cheary, A. A. Coelho, and J. P. Cline, "Fundamental Parameters Line Profile Fitting in Laboratory Diffractometers," *Journal of Research of the National Institute of Standards and Technology* 109 (2004): 1–25.

81. A. A. Coelho, "A Charge-flipping Algorithm Incorporating the Tangent Formula for Solving Difficult Structures," *Acta Crystallographica Section A, Crystal Physics, Diffraction, Theoretical and General Crystallography* 63 (2007): 400–406, https://doi.org/10.1107/S0108767307036112.

82. A. A. Coelho, "Whole-profile Structure Solution From Powder Diffraction Data Using Simulated Annealing," *Journal of Applied Crystallography* 33 (2000): 899–908.

83. H. M. Rietveld, "A Profile Refinement Method for Nuclear and Magnetic Structures," *Journal of Applied Crystallography* 2 (1969): 65–71.

84. *Origin Pro 2024 (version 10.1.0.170)*, OriginLab Corporation, Northampton, MA (USA), 2024.

85. *CorelDRAW Graphics Suite 2017 (version 19.0.0.328)*, Corel Corporation, Ottawa, Ontario (Canada), 2017.

86. G. Kresse and J. Furthmüller, "Efficiency of Ab-initio Total Energy Calculations for Metals and Semiconductors Using a Plane-wave Basis Set," *Computational Material Science* 6 (1996): 15–50.

87. G. Kresse and J. Furthmüller, "Efficient Iterative Schemes for Ab Initio Total-energy Calculations Using a Plane-wave Basis Set," *Physical Review B* 54 (1996): 11169–11186.

88. G. Kresse and J. Hafner, "*Ab Initio* Molecular Dynamics for Liquid Metals," *Physical Review B* 47 (1993): 558–561.

89. G. Kresse and D. Joubert, "From Ultrasoft Pseudopotentials to the Projector Augmented-wave Method," *Physical Review B* 59 (1999): 1758–1775.

90. J. P. Perdew, A. Ruzsinszky, G. I. Csonka, et al., "Restoring the Density-gradient Expansion for Exchange in Solids and Surfaces," *Physical Review Letters* 100 (2008): 136406, https://doi.org/10.1103/PhysRevLett.100.136406.

91. J. P. Perdew, A. Ruzsinszky, G. I. Csonka, et al., "Erratum: Restoring the Density-Gradient Expansion for Exchange in Solids and Surfaces [Phys. Rev. Lett. 100, 136406 (2008)]," *Physical Review Letters* 102 (2009): 039902, https://doi.org/10.1103/PhysRevLett.102.039902.

92. P. E. Blöchl, "Projector Augmented-wave Method," *Physical Review B* 50 (1994): 17953–17979.

93. S. Grimme, S. Ehrlich, and L. Goerigk, "Effect of the Damping Function in Dispersion Corrected Density Functional Theory," *Journal of Computational Chemistry* 32 (2011): 1456–1465, https://doi.org/10.1002/jcc.21759.

94. G. M. Sheldrick, "SHELXT—integrated Space-group and Crystal-structure Determination," *Acta Crystallographica Section A, Crystal Physics, Diffraction, Theoretical and General Crystallography* 71 (2015): 3–8, https://doi.org/10.1107/S2053273314026370.

95. O. V. Dolomanov, L. J. Bourhis, R. J. Gildea, J. A. K. Howard, and H. Puschmann, "OLEX2: A Complete Structure Solution, Refinement and Analysis Program," *Journal of Applied Crystallography* 42 (2009): 339–341, https://doi.org/10.1107/S0021889808042726.

96. Bruker AXS *Saint V8.40B* (2012).

97. Bruker AXS *APEX 5 v2023.9-2* (Bruker AXS Inc., 2023).

15213773, 2026, 45, Downloaded from https://onlinelibrary.wiley.com/doi/10.1002/anie.430417 by Universitatsbibliothek Augsburg, Wiley Online Library on [08/11/2026]. See the Terms and Conditions (https://onlinelibrary.wiley.com/terms-and-conditions) on Wiley Online Library for rules of use; OA articles are governed by the applicable Creative Commons License

98. L. Krause, R. Herbst-Irmer, G. M. Sheldrick, and D. Stalke, "Comparison of Silver and Molybdenum Microfocus X-ray Sources for Single-crystal Structure Determination," *Journal of Applied Crystallography* 48 (2015): 3–10, https://doi.org/10.1107/S1600576714022985.

Supporting Information

Additional supporting information can be found online in the Supporting Information section.

A detailed description of the experimental as well as computational methodology is provided in the Supporting information. The authors have cited additional references within the Supporting Information [66, 67, 73–98].

Supporting File: anie74838-sup-0001-SuppMat.pdf.

15213773, 2026, 45, Downloaded from https://onlinelibrary.wiley.com/doi/10.1002/anie.433004117 by Universitätsbibliothek Augsburg, Wiley Online Library on [08/11/2026]. See the Terms and Conditions (https://onlinelibrary.wiley.com/terms-and-conditions) on Wiley Online Library for rules of use; OA articles are governed by the applicable Creative Commons License